Applied Mathematics and Computation 219 (2012) 3993–4005

Contents lists available at SciVerse ScienceDirect

Applied Mathematics and Computation

journal homepage: www.elsevier.com/locate/amc

Axisymmetric magneto-hydrodynamic (MHD) flow and heat transfer at a non-isothermal stretching cylinder

K. Vajravelu [a,*], K.V. Prasad [b,1], S.R. Santhi [b]

[a] Department of Mathematics, Department of Mechanical, Material and Aerospace Engineering, University of Central Florida, Orlando, FL 32816, USA
[b] Department of Mathematics, Bangalore University, Bangalore 560001, India

ARTICLE INFO

Keywords:
Axisymmetric flow
Non-isothermal stretching cylinder
Variable thermal conductivity
Internal heat generation/absorption
Heat transfer
Finite difference method

ABSTRACT

An investigation is made to study the effects of transverse curvature and the temperature dependent thermal conductivity on the magneto-hydrodynamic (MHD) axisymmetric flow and heat transfer characteristics of a viscous incompressible fluid induced by a non-isothermal stretching cylinder in the presence of internal heat generation/absorption. It is assumed that the cylinder is stretched in the axial direction with a linear velocity and the surface temperature of the cylinder is subjected to vary non-isothermally. Here the thermal conductivity is assumed to vary linearly with temperature. Using a similarity transformation, the governing system of partial differential equations is first transformed into coupled non-linear ordinary differential equations with variable coefficients. The resulting intricate non-linear boundary value problem is solved numerically by a second order finite difference scheme for different values of the pertinent parameters for two cases: (i) the prescribed surface temperature (PST case) and (ii) the prescribed heat flux (PHF case). Numerical results are obtained for two different cases namely, zero and non-zero values of the curvature parameter to get the effects on the velocity and temperature fields. The combined effects of the curvature parameter and the thermal conductivity parameter are examined. The physical significances of the numerical results are presented for several limiting cases.

1. Introduction

The study of boundary layer flow and heat transfer at a stretching surface is important in manufacturing and technological processes. For example, heat treated materials traveling between a feed roll and a wind-up roll, aerodynamic extrusion of plastic sheets, glass fiber and paper production, cooling of an infinite metallic plate in a cooling bath, and manufacturing of polymeric sheets, etc. (see Altan et al. [1], Fisher [2] and Tadmor and Klein [3]). In particular, extradite from a die is drawn and simultaneously stretched into a sheet, which is then solidified through quenching or by gradual cooling by direct contact with water. The quality of the final product depends on the rate of heat transfer at the stretching surface. In view of these applications, Crane [4] was the first among others to obtain an elegant analytical solution to the boundary layer equations for the two-dimensional flow due to a stretching surface in a quiescent incompressible fluid. Since then, many authors (Gupta and Gupta [5], Rajagopal et al. [6], Siddappa and Abel [7], Grubka and Bobba [8] and Ali [9]) have considered various aspects of the problem and obtained similarity solutions. A similarity solution is the one in which number of independent variables are reduced, at least one, by a coordinate transformation. Despite the growth of the boundary layers with distance from the

* Corresponding author.
E-mail address: kuppalapalle.vajravelu@ucf.edu (K. Vajravelu).
[1] Present address: Department of Mathematics, Vijayanagara Sri Krishnadevaraya University, Vinayaka Nagar, Bellary 583 104, Karnataka, India.

0096-3003/$ - see front matter © 2012 Elsevier Inc. All rights reserved.
http://dx.doi.org/10.1016/j.amc.2012.10.034

Nomenclature

a	radius of the cylinder
b	stretching rate parameter
B_0	uniform magnetic field
$c_1,\ c_2,\ c_3,\ c_4$	constants
c_p	specific heat at constant pressure
C_f	skin friction coefficient
f	dimensionless stream function
g	dimensionless temperature in PHF case
k_w	thermal conductivity at the wall
k_∞	conductivity of the fluid far away from the cylinder
l	reference length
M	Kummer's function
Mn	magnetic parameter
m	constant
Pr	Prandtl number
q_w	surface heat flux
$p_0,\ q_0,\ p_1,\ q_1$	constants
Q	dimensional heat generation/absorption
r	radial coordinate
Re_x	local Reynolds number
s, t	temperature exponent
T	fluid temperature
T_w	temperature of the cylinder surface
T_∞	ambient temperature
u	axial velocity component
U_w	stretching velocity
v	radial velocity component
x	axial coordinate

Greek symbols

$\alpha(T)$	temperature-dependent thermal diffusivity
α_∞	diffusivity far away from the wall
β	heat source/sink parameter
γ	transverse curvature
η	similarity variable
θ	dimensionless temperature in PST case
ν	kinematic viscosity
τ_w	surface shear stress
ρ	density
σ	electric conductivity
ψ	stream function
ε	variable thermal conductivity

Subscripts

w	conditions at the stretching sheet
∞	condition at infinity

Superscript

$'$	differentiation with respect to η

leading edge, the velocity and temperature profiles remain geometrically similar. The boundary layer flow and heat transfer due to a stretching surface in a quiescent viscous fluid with hydromagnetic effects are considered by Sarpakaya [10], Pavlov [11], Chakrabarti and Gupta [12], Prasad and Vajravelu [13], Abel et al. [14] and Cortell [15]. The results of these studies have applications to polymer technology related to the stretching of plastic sheets. Also, many metallurgical processes involve the cooling of continuous strips or filaments by drawing them through a quiescent fluid and while drawing these strips are sometimes stretched. The rate of cooling can be controlled by drawing such strips in an electrically conducting fluid subjected to a transverse magnetic field in order to get the final products of desired characteristics.

All the above investigators restricted their analyses to two-dimensional flow and heat transfer problems over a stretching sheet. But not much is being done for the much more intricate problem of the axisymmetric flow due to a stretching cylinder. Flow over cylinders is considered to be two dimensional when the radius of the cylinder is large compared to the boundary layer thickness. On the other hand, for a thin cylinder, the radius may be of the same order as the boundary layer thickness. Therefore, the flow may be considered as axisymmetric instead of two-dimensional. In this case, the governing equations contain the transverse curvature term which may affect the velocity and temperature fields. The effect of the transverse curvature is important in certain technological applications such as hot rolling, wire or fiber drawing where accurate prediction of flow and heat transfer is required and thick boundary layer can exist on slender or near slender bodies. In view of this, Crane [16] studied the boundary layer flow due to a stretching cylinder. Wang [17] extended the work of Crane [16] to study the flow of a viscous fluid at a stretching hollow cylinder in an ambient fluid at rest. The problem is governed by a third order nonlinear ordinary differential equation that leads to an exact similarity solution for the Navier stokes equations. Pop et al. [18] investigated the boundary layer flow past a moving longitudinal cylinder in a non-Newtonian power law fluid at rest. Bachok and Ishak [19] analyzed the effects of the governing parameters on the flow and heat transfer over a horizontal cylinder with prescribed surface heat flux. In all these studies, the thermo-physical properties are assumed to be constant. However, it is well known that these properties may change with temperature, especially the thermal conductivity. Available literature on variable thermal conductivity (Chiam [20], Datti et al. [21], Prasad and Vajravelu [13]) shows that not much work is being done for the axisymmetric flow over a stretching cylinder.

In view of this, the present authors study, in this paper, the effects of the temperature dependent thermal conductivity on the axisymmetric magneto-hydrodynamic (MHD) flow and heat transfer over a non-isothermal stretching cylinder in the presence of internal heat generation/absorption. In contrast to the work of Bachok and Ishak [19], here the thermal conductivity varies with temperature, as this is true in the case of polymer solutions; this leads to non-linearity in the boundary value problem (Savvas et al. [22]). Also, in this study, we consider the following two different types of the non-isothermal boundary conditions, namely:

(i). the surface with prescribed power law temperature distribution (PST case); and
(ii). the surface with prescribed power law heat flux (PHF case), varying linearly with the distance

In addition to this, we also consider the endothermic/exothermic chemical reactions (by including the effect of internal heat generation/absorption in the energy equation). Due to the influence of the transverse curvature and the temperature dependent thermal conductivity, the momentum and energy equations are coupled and highly non-linear. Using a similarity transformation, the governing system of partial differential equations is first transformed into coupled non-linear ordinary differential equations with variable coefficients. The resulting boundary value problem is solved numerically by a second order finite difference scheme known as the Keller-box method.

2. Flow analysis

Let us consider a steady, the exterior viscous, incompressible and electrically conducting fluid flow due to the extrusion of a long impermeable hollow horizontal cylinder with a constant radius a. The x-axis is measured along the axis of the cylinder and r-axis is measured in the radial direction as shown in Fig. 1 (see Wang [17]). A uniform magnetic field of strength B_0 is applied in the radial direction. The magnetic Reynolds number is assumed to be small so that the induced magnetic field is neglected in comparison with the applied magnetic field. Also, applied electric field, the Hall current and the Joule heating are neglected. Under these assumptions, along with the usual boundary layer approximation, the governing equations for the flow are

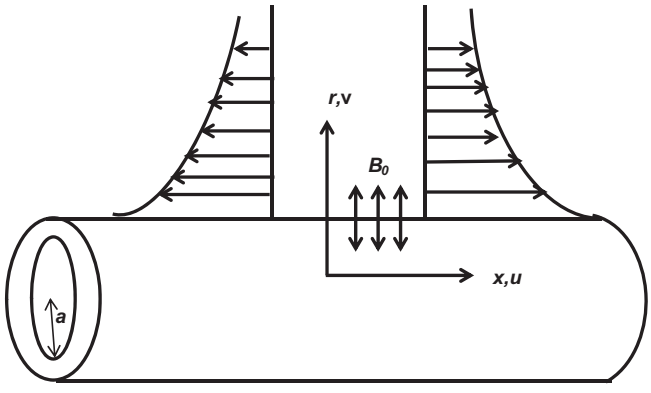

Fig. 1. Physical model and co-ordinate system.

$$\frac{\partial}{\partial x}(ru)+\frac{\partial}{\partial r}(rv)=0, \tag{1}$$

$$u\frac{\partial u}{\partial x}+v\frac{\partial u}{\partial r}=\nu\left(\frac{\partial^2 u}{\partial r^2}+\frac{1}{r}\frac{\partial u}{\partial r}\right)-\frac{\sigma B_0^2 u}{\rho}, \tag{2}$$

where u and v are the fluid velocity components measured along x and r respectively. Here, ν is the kinematic viscosity, σ is the electrical conductivity, B_0 is the transverse magnetic field, and ρ is the density. The appropriate boundary conditions to this problem are

$$u=U_w,\quad v=0\quad \text{at } r=a\quad \text{and}\quad u\to 0\quad \text{as } r\to\infty. \tag{3}$$

Here $U_w=b(x/l)$ is the stretching velocity, $b>0$ is the stretching rate and l is the reference length. The governing Eq. (2) in terms of stream function ψ, where ψ satisfies $(u,v)=\left(\frac{1}{r}\frac{\partial\psi}{\partial r},-\frac{1}{r}\frac{\partial\psi}{\partial x}\right)$ can be written as

$$\nu\left(\frac{1}{r^2}\frac{\partial\psi}{\partial r}-\frac{1}{r}\frac{\partial^2\psi}{\partial r^2}+\frac{\partial^3\psi}{\partial r^3}\right)-\left(\frac{1}{r}\frac{\partial^2\psi}{\partial x\partial r}+\frac{1}{r^2}\frac{\partial\psi}{\partial x}+\frac{\sigma B_0^2}{\rho}\right)\frac{\partial\psi}{\partial r}+\frac{1}{r}\frac{\partial\psi}{\partial x}\frac{\partial^2\psi}{\partial r^2}=0. \tag{4}$$

The stream function ψ automatically satisfies the continuity Eq. (1). Following Ishak and Nazar [23], we define η and ψ as

$$\eta=\frac{r^2-a^2}{2a}\left(\frac{U_w}{\nu x}\right)^{\frac{1}{2}},\quad \psi=(\nu x U_w)^{\frac{1}{2}}af(\eta), \tag{5}$$

where f is the dimensionless variable and η is the similarity variable. By defining η in this form, the boundary condition at $r=a$ reduce to the boundary condition at $\eta=0$, which is more convenient for numerical computations. From Eq. (5), we obtain

$$u=U_w f'(\eta),\quad v=-\frac{a}{r}\left(\frac{\nu b}{l}\right)^{\frac{1}{2}}f(\eta), \tag{6}$$

here prime denotes differentiation with respect to η. Substituting Eqs. (5) and (6) in Eqs. (2) and (3), we obtain

$$((1+2\eta\gamma)f'')'-(f')^2+ff''-Mn\quad f'=0 \tag{7}$$

and

$$f(0)=0,\quad f'(0)=1\quad \text{and}\quad f'(\infty)=0. \tag{8}$$

The parameters γ and Mn are the transverse curvature and the magnetic parameter respectively and they are defined by

$$\gamma=\sqrt{\frac{l\nu}{ba^2}}\quad \text{and}\quad Mn=\frac{\sigma B_0^2 l}{\rho b}. \tag{9}$$

Further we noticed that when $\gamma=0$ (flat plate), Eq. (7) reduces to those considered by Crane [4] where the closed-form solution is given by

$$f=\frac{1-e^{-mn\eta}}{m}\quad \text{where } m=\sqrt{1+Mn}, \tag{10}$$

where m is the constant. The skin friction coefficient C_f at the surface of the cylinder is given by

$$C_f=\frac{2\tau_w}{\rho_\infty U_w^2}=2f''(0)(\mathrm{Re}_x)^{-1/2}, \tag{11}$$

where the surface shear stress is defined by $\tau_w=\mu\left(\frac{\partial u}{\partial r}\right)_{r=a}=\mu U_w\sqrt{\frac{U_w}{\nu x}}f''(0)$ with μ is the dynamic viscosity and $\mathrm{Re}_x=U_w x/\nu$ is the local Reynolds number. We now discuss the heat transport in the above axisymmetric flow due to a stretching cylinder.

3. Heat analysis

The energy equation for the fluid with variable thermal conductivity in the presence of internal heat generation / absorption for axisymmetric flow is given by Chiam [20]

$$u\frac{\partial T}{\partial x}+v\frac{\partial T}{\partial r}=\frac{1}{r}\frac{\partial}{\partial r}\left(\alpha(T)r\frac{\partial T}{\partial r}\right)+\frac{Q}{\rho c_p}(T-T_\infty), \tag{12}$$

where T is the temperature of the fluid, c_p is the specific heat at constant pressure, and $\alpha(T)$ is the temperature dependent thermal diffusivity, which is assumed to vary as a linear function of temperature. It is further assumed that the surface of the cylinder is maintained at a variable temperature T_w and the ambient fluid temperature at T_∞. The last term containing Q in

Eq. (12) represents the temperature-dependent volumetric heat source when $Q > 0$ and heat sink when $Q < 0$; dealing with the situation of exothermic and endothermic chemical reactions, respectively. Here, the thermal boundary conditions depend on the type of heating processes under consideration. We consider two different heating processes namely, (1) prescribed surface temperature (PST) and (2) prescribed wall heat flux (PHF). The heat transfer analysis for these two processes is carried out in Sections 3.1 and 3.2.

3.1. Prescribed surface temperature (PST case)

For this circumstance, the boundary conditions are

$$T = T_w[= T_\infty + c_1(x/l)^s] \quad \text{at } r = a \quad \text{and} \quad T \to T_\infty \quad \text{as } r \to \infty, \tag{13}$$

where c_1 is the constant and s is the temperature exponent, we assume that thermal diffusivity $\alpha(T)$ in the form (Chiam [20] and Datti et al. [21])

$$\alpha(T) = \alpha_\infty(1 + \varepsilon\theta(\eta)), \quad \varepsilon = (k_w - k_\infty)/k_\infty \quad \text{and} \quad \theta(\eta) = (T - T_\infty)/(T_w - T_\infty), \tag{14}$$

where ε is a small parameter depending on the nature of the fluid, α_∞ is the thermal diffusivity, k_w is the thermal conductivity at the surface of the cylinder, k_∞ is the thermal conductivity of the fluid far away from the cylinder and θ is the dimensionless temperature. Using Eqs. (6) and (14), Eqs. (12) and (13) becomes

$$(1 + 2\eta\gamma)((1 + \varepsilon\theta)\theta')' + 2(1 + \varepsilon\theta)\gamma\theta' - \Pr(sf'\theta - f\theta') + \Pr\beta\theta = 0, \tag{15}$$

and

$$\theta(0) = 1 \quad \text{and} \quad \theta(\infty) = 0. \tag{16}$$

Here, the parameters Pr and β are the Prandtl number, and the heat source/sink parameter, respectively and they are defined as

$$\Pr = \frac{\nu}{\alpha_\infty} \quad \text{and} \quad \beta = \frac{Ql}{b\rho c_p}. \tag{17}$$

3.2. Prescribed heat flux (PHF case)

In this case, the boundary conditions are

$$-k_\infty \frac{\partial T}{\partial r} = q_w = c_2(x/l)^t \quad \text{at } r = a \quad \text{and} \quad T \to T_\infty \quad \text{as } r \to \infty, \tag{18}$$

where c_2 is the constant and t is the temperature exponent, we consider that thermal diffusivity $\alpha(T)$ in the form (Chiam [20] and Datti et al. [21])

$$\alpha(T) = \alpha_\infty(1 + \varepsilon g(\eta)), \quad g(\eta) = (T - T_\infty)/(T_w - T_\infty) \quad \text{and} \quad T_w - T_\infty = (c_2/k_\infty)(x/l)^t\sqrt{vx/U_w}, \tag{19}$$

here g is the dimensionless temperature. Using Eqs. (6) and (19), Eqs. (12) and (18) becomes

$$(1 + 2\eta\gamma)((1 + \varepsilon g)g')' + 2(1 + \varepsilon g)\gamma g' - \Pr(tf'g - g\theta') + \Pr\beta g = 0, \tag{20}$$

subjected to the boundary conditions

$$g'(0) = -1 \quad \text{and} \quad g(\infty) = 0, \tag{21}$$

Here g is the dimensionless temperature.

4. Exact solutions for some special cases

Here, we present exact solutions in certain special cases: Such solutions are useful and serve as baseline results for comparison with the solutions obtained via the numerical scheme.

4.1. Perturbation analysis in the absence of transverse curvature

We follow a perturbation expansion approach to solve Eq. (15) (PST case). Suppose

$$\theta(\eta) = \theta_0(\eta) + \varepsilon\theta_1(\eta) + \varepsilon^2\theta_2(\eta) + \cdots. \tag{22}$$

Substituting this into Eq. (15) and equating like powers of ε ignoring quadratic and higher order terms in ε, we obtain

$$\theta_0'' + \Pr f\theta_0' - \Pr(sf' - \beta)\theta_0 = 0, \tag{23}$$

with boundary conditions

$$\theta_0(0) = 1, \quad \theta_0(\infty) = 0.$$

and

$$\theta_1'' + \mathrm{Pr} f \theta_1' - \mathrm{Pr}(sf' - \beta)\theta_1 = -\theta_0\theta_0'' - \theta_0'^2, \tag{24}$$

with the boundary conditions

$$\theta_1(0) = 0, \quad \theta_1(\infty) = 0.$$

Equation for θ_0 can be solved explicitly in terms of Kummer's function (Abramowitz and Stegun [24]) and is given by

$$\theta_0(\eta) = c_3 \exp(-m(p_0 + q_0)\eta/2) M(p_1, q_1; z),$$

where $M(p, q; z)$ denotes the confluent hypergeometric function,

$$1/c_3 = M(p_1, q_1; -\mathrm{Pr}/m^2), \quad p_1 = (p_0 + q_0 - 2s)/2 \quad \text{and} \quad q_1 = 1 + q_0.$$
$$p_0 = \mathrm{Pr}/m^2, \quad q_0 = p_0\sqrt{1 - (4\beta/p_0)}, \quad z = -(\mathrm{Pr}/m^2)\exp(-m\eta),$$

A similar analysis can be carried out for Eq. (20) for the PHF case. We have

$$g_0(\eta) = c_4 \exp(-m(p_0 + q_0)\eta/2) M(p_1, q_1; z)$$

$$\text{where } g(\eta) = g_0(\eta) + \varepsilon g_1(\eta) + \varepsilon^2 g_2(\eta) + \cdots$$

$$1/c_4 = (m(p_0 + q_0)/2) M(p_1, q_1; -\mathrm{Pr}/m^2) - (p_1 \mathrm{Pr}/q_1 m) M(p_1 + 1, q_1 + 1; -\mathrm{Pr}/m^2).$$

We now analyse Eq. (24) (PST case), which gives the first-order correction term $\varepsilon\theta_1$. Note that Eq. (24) is linear and inhomogeneous and therefore it is possible to obtain a power series solution for θ_1 However, it becomes very tedious to obtain various values of θ_1 using this power series solution. Instead, we employ the second order finite difference scheme. Similar procedure is applied to the PHF case also. The local wall heat flux can be expressed as

$$q_w = -k_\infty \left(\frac{\partial T}{\partial r}\right)_{r=a} = -k_\infty c_1 (x/l)^s \sqrt{\frac{U_w}{\nu x}} \theta'(0),$$

and the wall temperature T_w is obtained from Eq. (19) as

$$T_w - T_\infty = (c_2/k_\infty)(x/l)^t \sqrt{\nu x/U_w} g(0).$$

5. Numerical method

The axisymmetric flow and heat transfer of the impermeable hollow horizontal cylinder is affected by non-dimensional parameters, namely, the transverse curvature, the magnetic parameter, the internal heat source/sink parameter, the temperature exponent parameter, the Prandtl number and the variable thermal conductivity parameter. The system of coupled nonlinear equations (7), (15), and (20) with variable coefficients subject to the boundary conditions (8), (16), and (21) is solved numerically by an implicit finite difference scheme known as the Keller box method (see for details Cebeci and Bradshaw [25], Keller [26] and Prasad and Vajravelu [13]). The numerical solutions are obtained in four steps as follows:

- reduce Eqs.(7), (15), and (20) to a system of first-order equations;
- write the difference equations using central differences;
- linearize the algebraic equations by Newton's method, and write them in matrix–vector form; and
- solve the linear system by the block tri-diagonal elimination technique.

The step size $\Delta\eta$ and the position of the edge of the boundary layer η_∞ are to be adjusted for different values of the parameters to maintain accuracy. For brevity, the details of the solution procedure are not presented here. It is also important to note that the computational time for each set of input parametric values should be short. Because physical domain in this problem is unbounded, whereas the computational domain has to be finite, we apply the far field boundary conditions for the similarity variable η at finite value denoted by $\eta_{\max}$. We ran our bulk of computations with the value $\eta_{\max} = 12$, which is sufficient to achieve the far field boundary conditions asymptotically for all values of the parameters considered.

Here the boundary layer flow and heat transfer of the non-isothermal stretching cylinder is affected by the transverse curvature parameter, the magnetic parameter, the internal heat source/sink parameter, the temperature exponent parameter and the variable thermal conductivity parameter. The main focus of the present study is to bring out the effects of these major parameters through the numerical solutions of the boundary value problem through the skin friction, the wall temperature gradient in PST case and wall temperature in PHF cases. For numerical calculations, a uniform step size of $\Delta\eta = 0.01$ is found to be satisfactory and the solutions are obtained with an error tolerance of 10^{-6} in all the cases. The accuracy of the

Table 1
Comparison of some of the values of $-f''(0)$ for different values of Mn when $\gamma = 0$.

	Mn = 0.0	Mn = 0.5	Mn = 1.0	Mn = 1.5	Mn = 2.0
Numerical solution by Keller-box method	1.000001	1.224745	1.414214	1.581139	1.732051
Analytical solution	1.000000	1.224745	1.414214	1.581139	1.732051

Table 2
Comparison of some of the values of wall temperature gradient in PST case and wall temperature in PHF case with the present results for $\varepsilon = 0$, $\beta = 0$ and $s = 1.0$.

Pr	$\gamma = 0$, PHF case				$\gamma = 1$, PHF case	
	Elbashbeshy [27]	Liu [28]	Bachok and Ishak [19]	Present values	Bachok and Ishak [19]	Present values
0.72	1.2253		1.2367	1.236657	0.8701	0.870057
1	1.0000		1.0000	1.000000	0.7439	0.743867
6.7		0.333303	0.3333	0.333304	0.2966	0.296555
10	0.2688		0.2688	0.268760	0.2442	0.244155
	$\gamma = 0$, PST case					
	Grubka & Bobba [8]		Ali [9]	Ishak and Nazar [23]		Present values
1	1.0000		0.9961	1.0000		1.00002
10	3.7207		3.7006	3.7207		3.72078

numerical scheme has been validated by comparing the skin friction, the wall temperature gradient and wall temperature with the available results in the literature, and found to be in very good agreement (Tables 1 and 2).

6. Results and discussion

The numerical computation has been carried out for different values of the magnetic parameter Mn, the transverse curvature γ, the Prandtl number Pr, the variable thermal conductivity parameter ε, the temperature exponent parameter and the heat source/sink parameter β. In order to get a clear insight into the physical problem, the horizontal velocity profiles and

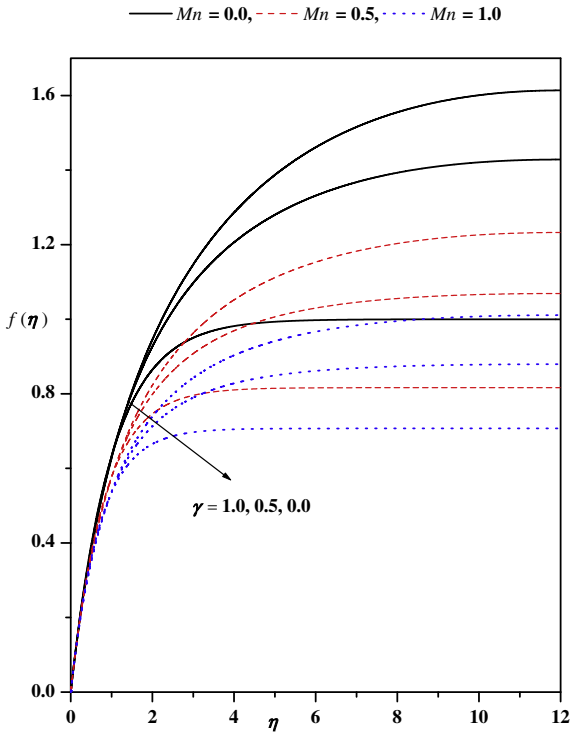

Fig. 2. (a) Transverse velocity profile for different values of γ and Mn (b). Horizontal velocity profile for different values of γ and Mn.

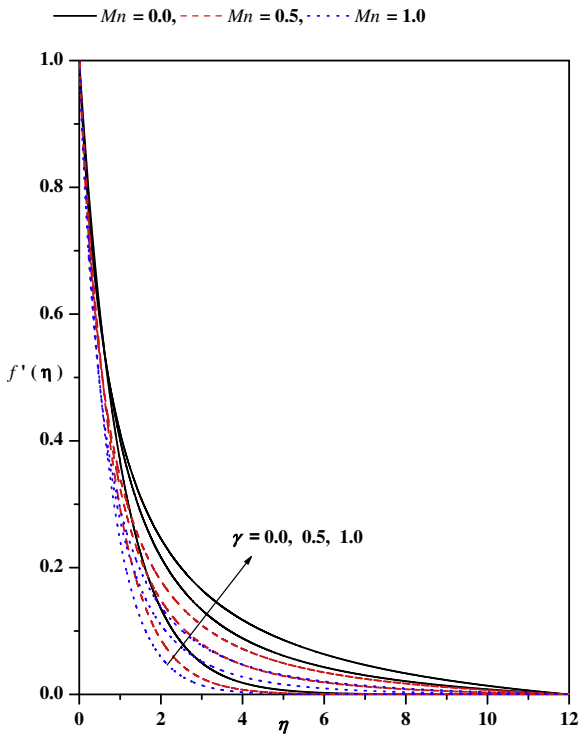

Fig. 2. (*continued*)

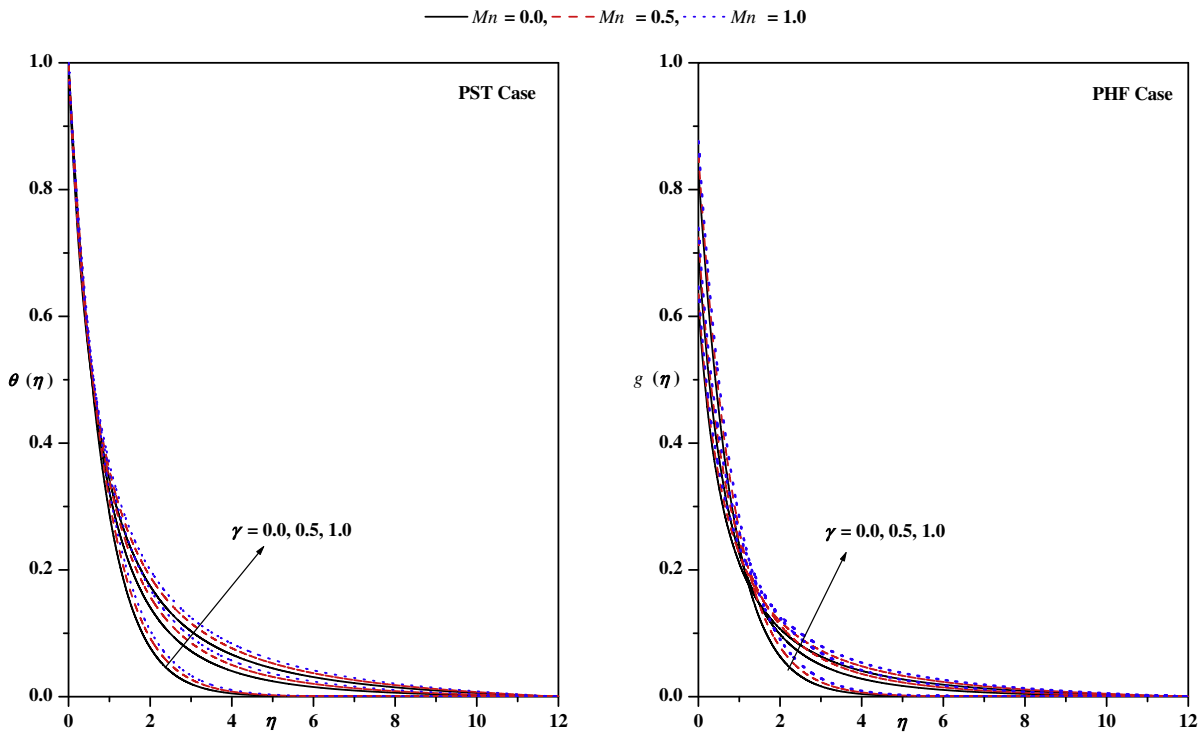

Fig. 3. Temperature profile for different values of γ and Mn when Pr = 1.0, $\varepsilon = 0.1$, $\beta = -0.5$ and $s = t = 1.0$; (a) PST case and (b) PHF case.

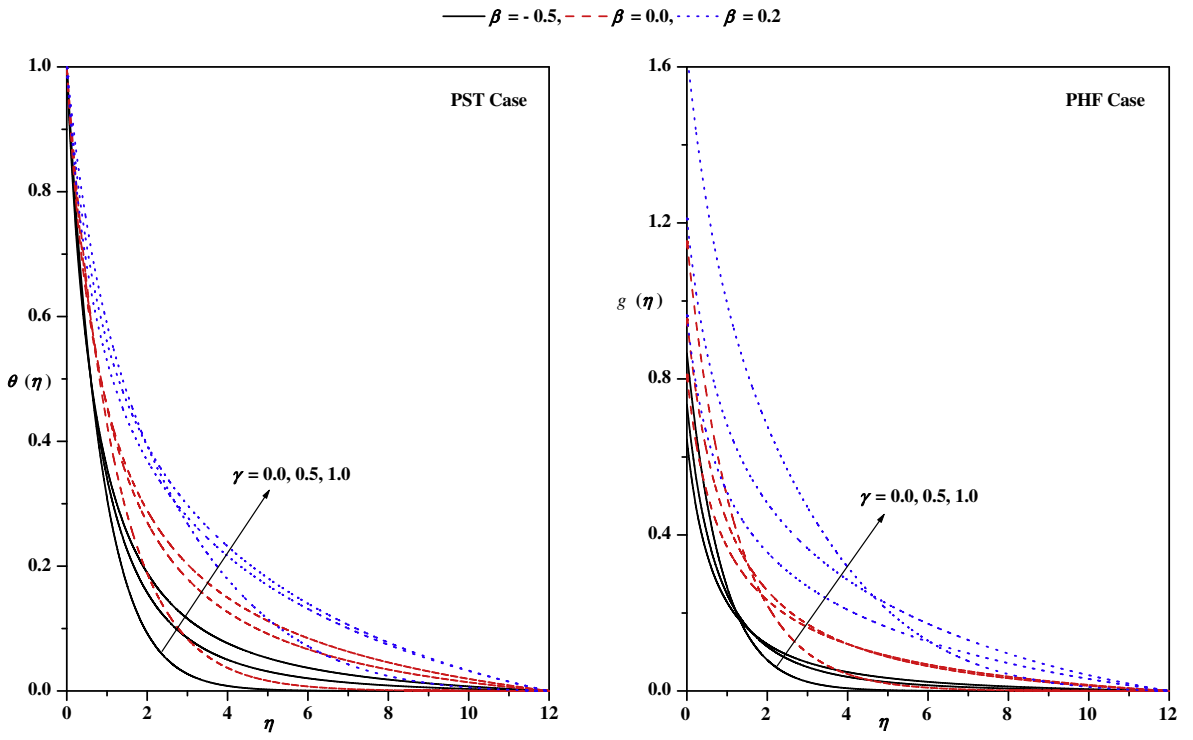

Fig. 4. Temperature profile for different values of γ and β when $Mn = 0.5$, $\varepsilon = 0.1$, Pr = 1.0 and $s = t = 1.0$; (a) PST case and (b) PHF case.

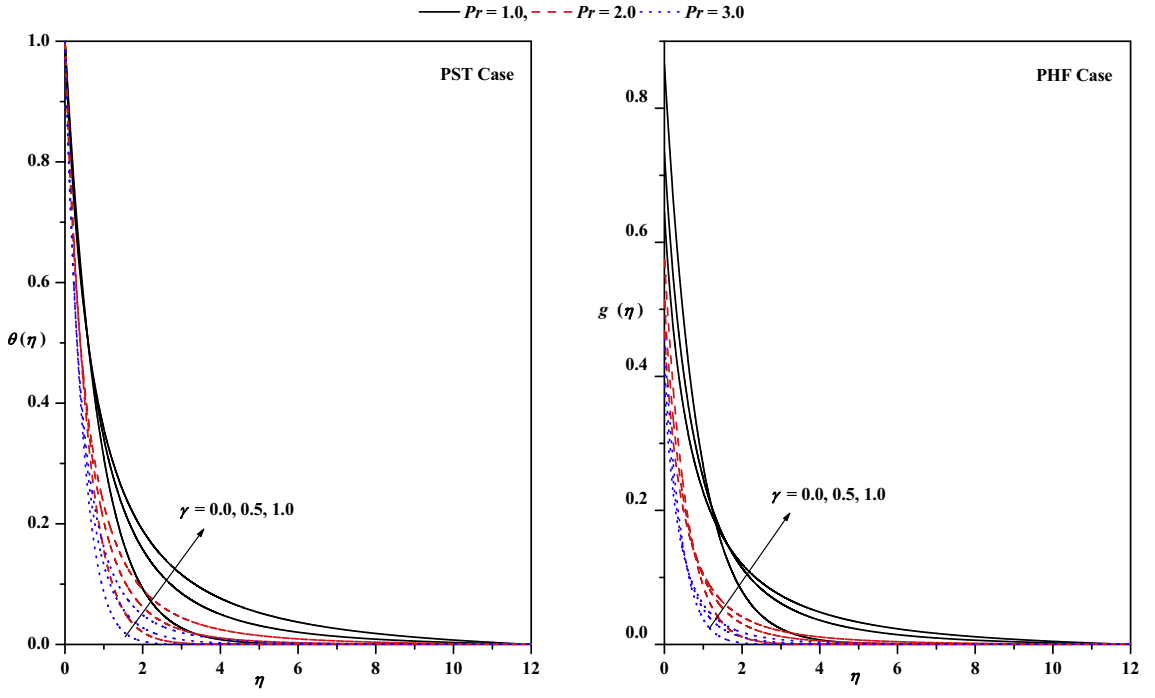

Fig. 5. Temparature profile for different values of γ and Pr when $Mn = 0.5$, $\varepsilon = 0.1$, $\beta = -0.5$ and $s = t = 1.0$; (a) PST case and (b) PHF case.

temperature profiles for both PST and PHF cases are discussed. The numerical results are shown graphically in Figs. 2–7. These figures depict the velocity profiles (Fig. 2(a) and (b)), and the temperature profiles (Figs. 3–7). Effects of the pertinent parameters on the skin friction, the wall temperature gradient in PST case and the wall temperature in PHF cases are tabulated in Tables 3 and 4.

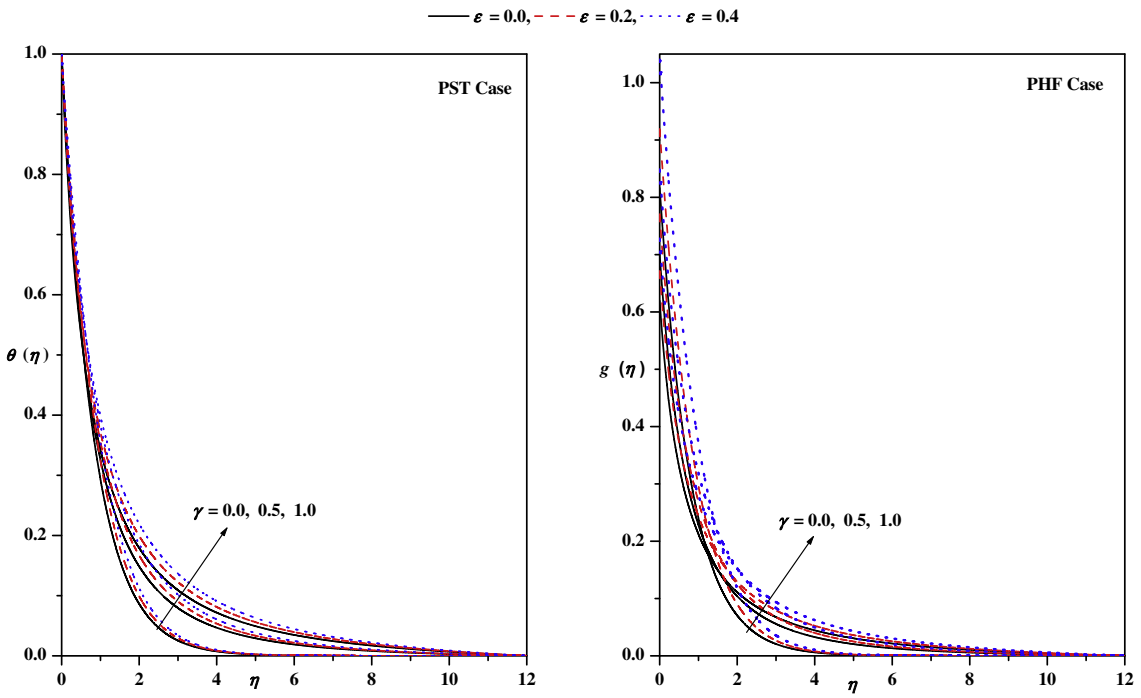

Fig. 6. Temperature profile for different values of γ and ε when Pr = 1.0, Mn = 0.5, $\beta = -0.5$ and $s = t = 1.0$; (a) PST case and (b) PHF case.

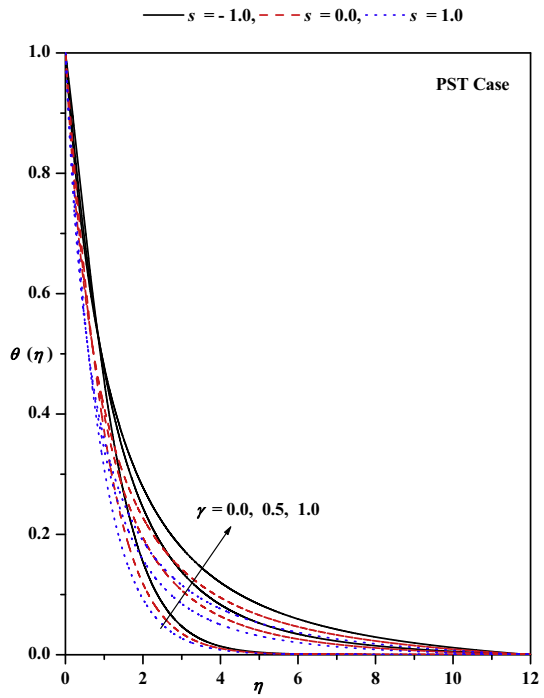

Fig. 7. (a) Temperature profile for different values of γ and s when Pr = 1.0, Mn = 0.5, $\beta = -0.5$ and $\varepsilon = 0.1$. (b) Temperature profile for different values of γ and t when Pr = 1.0, Mn = 0.5, $\beta = -0.5$ and $\varepsilon = 0.1$.

Fig. 2(a) and (b) illustrate the effects of the transverse curvature and the magnetic parameter Mn on the transverse velocity $f(\eta)$ and the horizontal velocity $f'(\eta)$. We notice from these figures that the transverse velocity profile decrease but the horizontal velocity profile increase with increasing values of the transverse curvature. The effect of increasing values of the

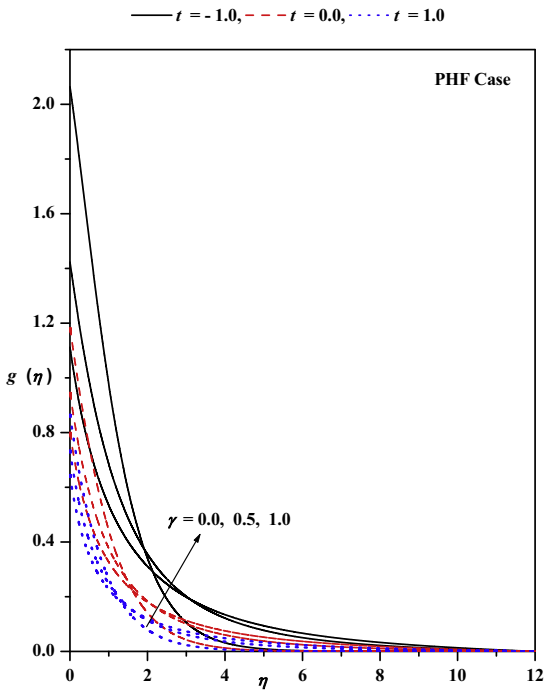

Fig. 7. (*continued*)

Table 3
Numerical values of skin-friction $-f''(0)$ for different values Mn and γ.

Mn	$\gamma = 0.0$	$\gamma = 0.25$	$\gamma = 0.5$	$\gamma = 0.75$	$\gamma = 1.0$
0.0	1.000001	1.091826	1.182410	1.271145	1.358198
0.5	1.224745	1.328505	1.427151	1.521975	1.613858
1.0	1.414214	1.523163	1.626496	1.725576	1.821302

Table 4
Numerical values of wall temperature gradient $-\theta'(0)$ in PST case and wall temperature $\theta(0)$ in PHF case for different values of the physical parameters.

s	Mn	Pr	ε	β	$-\theta'(0)$ PST case					$\theta(0)$ PHF case				
					$\gamma = 0.0$	$\gamma = 0.25$	$\gamma = 0.5$	$\gamma = 0.75$	$\gamma = 1.0$	$\gamma = 0.0$	$\gamma = 0.25$	$\gamma = 0.5$	$\gamma = 0.75$	$\gamma = 1.0$
1.0	0.5	1.0	0.1	−0.5	1.14511	1.24475	1.33936	1.43022	1.51822	0.86578	0.79307	0.73465	0.68620	0.64505
				0.0	0.87574	0.95685	1.04430	1.13157	1.21576	1.15389	1.04842	0.95485	0.87707	0.81209
				0.2	0.64562	0.71658	0.83662	0.93926	1.03488	1.63855	1.44304	1.21260	1.06939	0.96419
1.0	0.5	1.0	0.0	−0.5	1.22475	1.32851	1.42715	1.52198	1.61386	0.81650	0.75273	0.70070	0.65704	0.61963
			0.2		1.07758	1.17381	1.26505	1.35261	1.43738	0.91930	0.83624	0.77061	0.71683	0.67159
			0.4		0.96882	1.05972	1.14569	1.22807	1.30775	1.04031	0.93146	0.84859	0.78246	0.72794
1.0	0.5	1.0	0.1	−0.5	1.14511	1.24475	1.33936	1.43022	1.51822	0.86578	0.79307	0.73465	0.68620	0.64505
		2.0			1.69442	1.79278	1.88793	1.98020	2.06993	0.57424	0.54192	0.51397	0.48950	0.46785
		3.0			2.11925	2.21712	2.31262	2.40582	2.49688	0.45565	0.43522	0.41698	0.40060	0.38579
1.0	0.0	1.0	0.1	−0.5	1.17758	1.27923	1.37459	1.46562	1.55345	0.84061	0.77069	0.71503	0.66899	0.62991
	0.5				1.14511	1.24475	1.33936	1.43022	1.51822	0.86578	0.79307	0.73465	0.68620	0.64505
	1.0				1.11978	1.21909	1.31341	1.40414	1.49213	0.88651	0.81062	0.74982	0.69946	0.65675
−1.0	0.5	1.0	0.1	−0.5	0.51407	0.61944	0.71840	0.81300	0.90457	2.06440	1.67376	1.42314	1.24565	1.11179
0.0					0.85480	0.95663	1.05278	1.14487	1.23399	1.18338	1.04839	0.94691	0.86680	1.80133
1.0					1.14511	1.24475	1.33936	1.43022	1.51822	0.86578	0.79307	0.73465	0.68620	0.64505

transverse curvature is to increase the horizontal velocity and thereby enhance the boundary layer thickness. That is, the boundary layer thickness is higher for higher values of the transverse curvature, as clearly seen from Fig. 2(b). The velocity profiles show that the rate of transport is considerably reduced with the increase of *Mn*. It clearly indicates that the transverse magnetic field opposes the transport phenomena. This is due to the fact that variation of *Mn* leads to the variation of

the Lorentz force due to magnetic field, and the Lorentz force produces more resistance to transport phenomena. In all the cases considered, the velocity vanishes at some large distance from the surface of the tube.

The effects of the transverse curvature and the magnetic parameter on the temperature field in the boundary layer for both PST and PHF cases are shown in Fig. 3(a) and (b), respectively. It is observed that the temperature distribution is unity at the wall in PST case and is less than the unity at the wall in PHF case for all values of the transverse curvature. However, the temperature distribution for both PST and PHF cases decreases asymptotically to zero as the distance increases form the boundary layer. The effect of increasing the values of the transverse curvature parameter leads to accelerate the thermal boundary thickness. This behavior is true even for all values of the magnetic parameter, which in turn causes the enhancement of the temperature field. Figs. 4(a) and (b) exhibit the temperature distribution for different values of the curvature parameter and the heat source/sink parameter β for PST and PHF cases, respectively. From these figures, we observe that the temperature distribution is lower throughout the boundary layer for negative values of β (heat sink) and higher for positive values of β (heat source). Physically $\beta > 0$ implies $T_w > T_\infty$ i.e., the supply of heat to the flow region from the wall. Similarly, $\beta < 0$ implies $T_w < T_\infty$ i.e., the transfer of heat is from flow to the wall. The effect of an increase in the values of the heat source/sink parameter β is to increase the temperature for both PST and PHF cases. This holds for all values of the curvature parameter. The variations in the temperature for various values of the Prandtl number Pr are displayed in Fig. 5(a) and (b) for PST and PHF cases, respectively. Both of these figures demonstrate that an increase in the Prandtl number Pr results in a decrease in the temperature distribution, and tends to zero as the space variable increases from the wall. Also, the thermal boundary layer thickness decreases as the Prandtl number Pr increases for both PST and PHF cases.

The effects of the thermal conductivity parameter ε and the curvature parameter on the temperature are shown graphically in Fig. 6(a) and (b) for PST and PHF cases, respectively. The profiles demonstrate quite clearly that an increase in the value of ε results in an increase in the temperature and hence the thermal boundary layer thickness increase as ε increases. This is due to the fact that the assumption of temperature-dependent thermal conductivity causes a reduction in the magnitude of the transverse velocity by a quantity $\partial\alpha(T)/\partial r$, as can be seen from heat transfer Eqs. (15) and (20). This phenomenon holds for PHF case; however, thickness of the thermal boundary layer is thinner in comparison with PST case. For fixed values of the Prandtl number and the magnetic parameter, the effect of the surface temperature exponent parameter on the temperature profile for both PST and PHF cases are shown graphically in Fig. 7(a) and (b). From the graphical representation we observe that an increase in the temperature exponent parameter leads to decrease the temperature profile and hence the thermal boundary layer thickness decrease. This is due to the fact that, when $s > 0$, heat flows from the stretching cylinder to the ambient fluid and, when $s < 0$, the temperature gradient is positive and heat flows into the stretching cylinder from the ambient fluid. This behavior holds for PHF case also, as shown in Fig. 7(b).

The values of $-f''(0)$ which signify the local skin friction co-efficient, C_f, are recorded in Table 3 for different values of the physical parameters γ and Mn. From Table 3, we observe that the skin friction coefficient is negative for all values of the transverse curvature and the magnetic parameter. Physically, negative values of $f''(0)$ mean the surface exert a drag force on the fluid. This is not surprising since in the present problem, we consider the case of a stretching cylinder, which induces the flow. Since the Eqs. (7), (15), and (20) are uncoupled, the internal heat source/sink parameter, the temperature exponent parameter, the Prandtl number and the variable thermal conductivity parameter and the non-isothermal boundary conditions give no influence to the value of $f''(0)$. The absolute value of $f''(0)$ increases as the transverse curvature and the magnetic parameter increases: This result in an increase in the magnitude of the wall temperature gradient in PST case as well as in the PHF case for all the values of transverse curvature. Thus, the skin friction coefficient and the wall temperature gradient in the PST and the wall temperature in PHF cases are larger at a cylinder compared to that at a flat plate, which is observed by Grubka and Bobba [8] and Ali [9]. The effect of the magnetic parameter Mn is to increase the wall temperature gradient both in the PST and PHF cases. This is due to the fact that the thermal boundary layer decreases as the magnetic parameter Mn increases: This results in higher temperature gradient at the wall and hence higher heat transfer at the wall. The effect of increasing values of the variable thermal conductivity parameter and the heat source/sink parameter is to increase the wall temperature gradient; whereas the effect of the Prandtl number and the surface temperature exponent parameter is to decrease the wall temperature gradient. This observation is even true with wall temperature in the PHF case.

7. Conclusion

In this paper, we investigated the effect of transverse curvature on the axisymmetric flow and heat transfer of an electrically conducting fluid over a non-isothermal stretching cylinder with temperature dependent thermal conductivity in the presence of internal heat generation/absorption. The governing partial differential equations are transformed into a system of nonlinear ordinary differential equations with variable coefficients and then solved numerically by a second order finite difference scheme. A systematic study is made on the effects of the transverse curvature and the other physical parameters controlling the flow and heat transfer characteristics. The temperature profiles are obtained for two types of heating processes namely, the PST and the PHF cases for various values of the physical parameters. As expected, the transverse curvature parameter has the effect to increase the horizontal velocity and the temperature fields. Also, an increase in the value of magnetic parameter leads to a decrease in the velocity boundary layer thickness. However, quite the opposite is true with the thermal boundary layer thickness in both the PST and the PHF cases. It is worthy to note that the effect of increasing values of the heat source/sink parameter is to increase the temperature field in both the PST and the PHF cases. Finally, we conclude

that the thermal boundary layer thickness decreases with an increase in the Prandtl number and the surface temperature exponent parameter in both the PST and the PHF cases.

Acknowledgments

The authors appreciate the constructive comments of the reviewer which led to definite improvements in the paper. One of the authors (KVP) is thankful to the University Grants Commission, New Delhi for supporting financially under Major Research Project (Grant No. F. No. 41-790/2012 (SR)).

References

[1] T. Altan, S. Oh, H. Gegel (Metal Forming Fundamentals and Applications), American Society of Metals, Metals Park, OH, 1979.
[2] E.G. Fisher, Extrusion of Plastics, Wiley, New York, 1976.
[3] Z. Tadmor, I. Klein, Engineering Principles of Plasticating Extrusion, Polymer Science and Engineering Series, Van Nostrand Reinhold, New York, 1970.
[4] L.J. Crane, Flow past a stretching plate, ZAMP 21 (1970) 645–647.
[5] P.S. Gupta, A.S. Gupta, Heat and mass transfer on a stretching sheet with suction or blowing, Can. J. Chem. Eng. 55 (1977) 744–746.
[6] K.R. Rajagopal, T.Y. Na, A.S. Gupta, Flow of a visco-elastic fluid over a stretching sheet, Rheol. Acta. 23 (1984) 213.
[7] B. Siddappa, M.S. Abel, Non-Newtonian flow past a stretching plate, ZAMP 36 (1985) 47.
[8] L.G. Grubka, K.M. Bobba, Heat transfer characteristics of a continuous stretching surface with variable temperature, ASME J. Heat Transfer 107 (1985) 248–250.
[9] M.E. Ali, Heat transfer characteristics of a continuous stretching surface, Heat Mass Transfer 29 (1994) (1994) 227–234.
[10] T. Sarpakaya, Flow on non-Newtonian fluids in a magnetic field, Am. Inst. Chem. Eng. J. 7 (1961) 324.
[11] K.B. Pavlov, Magnetohydrodynamic flow of an incompressible viscous fluid caused by deformation of a plane surface, Magninaya Gidrodinamika (USSR) 4 (1974) 146.
[12] A. Chakrabarti, A.S. Gupta, Hydromagnetic flow and heat transfer over a stretching sheet, Quart. Appl. Math. 37 (1979) 73–78.
[13] K.V. Prasad, K. Vajravelu, Heat transfer in the MHD flow of a power law fluid over a non-isothermal stretching sheet, Int. J. Heat Mass Tranfer 52 (2009) 4956.
[14] M.S. Abel, A. Joshi, R, M. Sonth, Heat transfer in MHD visco-elastic fluid flow over stretching surface, ZAMM 81 (2001) 691–698.
[15] R. Cortell, A note on magneto hydrodynamic flow of a power-law fluid over a stretching sheet, Appl. Math. Comput. 168 (2005) 557–566.
[16] L.J. Crane, Boundary layer flow due to a stretching cylinder, ZAMP 26 (1975) 619–622.
[17] C.Y. Wang, Fluid flow due to a stretching cylinder, Phys. Fluids 31 (1988) 466.
[18] I. Pop, M. Kumari, G. Nath, Non-Newtonian boundary-layers on a moving cylinder, Int. J. Eng. Sci. 28 (1990) 303.
[19] N. Bachok, A. Ishak, Flow and heat transfer over a stretching cylinder with prescribed surface heat flux, Malays. J. of Math. Sci. 4 (2010) 159–169.
[20] T.C. Chiam, Heat transfer in a fluid with variable thermal conductivity over stretching sheet, Acta Mech. 129 (1998) 63–72.
[21] P.S. Datti, K.V. Prasad, M.S. Abel, A. Joshi, MHD visco-elastic fluid flow over a non-isothermal stretching sheet, Int. J. Eng. Sci. 42 (2004) 935–946.
[22] T.A. Savvas, N.C. Markatos, C. Papaspyrides, On the flow of non-Newtonian polymer solutions, Appl. Math. Model. 18 (1994) 14.
[23] A. Ishak, R. Nazar, Laminar boundary layer flow along a stretching cylinder, Euro. J. Sci. Res. 36 (2009) 22–29.
[24] M. Abramowitz, I.A. Stegun, Handbook of Mathematical Functions, Dover, New York, 1965.
[25] T. Cebeci, P. Bradshaw, Physical and Computational Aspects of Convective Heat Transfer, Springer-Verlag, NewYork, 1984.
[26] H.B. Keller, Numerical Methods for Two-Point Boundary Value Problems, Dover Publ., NewYork, 1992.
[27] E.M.A. Elbashbeshy, Heat transfer over a stretching surface with variable surface heat flux, J. Phys. D: Appl. Phy. 31 (1998) 1951–1954.
[28] I.C. Liu, A note on heat and mass transfer for a hydromagnetic flow over a stretching sheet, Int. Commun. Heat Mass Transfer 32 (2005) 1075–1084.